JOURNAL OF Materials CHEMISTRY

Investigation into the structures of binary-, tertiary- and quinternary-mixtures of *n*-alkanes and real diesel waxes using high-resolution synchrotron X-ray powder diffraction

Steven R. Craig,[a]† Gerard P. Hastie,[b] Kevin J. Roberts,[b]* Andrea R. Gerson,[a] John N. Sherwood[a] and Robert D. Tack[c]

[a]*Department of Pure and Applied Chemistry, University of Strathclyde, Glasgow, UK G1 1XL*
[b]*Centre for Molecular & Interface Engineering, Department of Mechanical and Chemical Engineering, Heriot-Watt University, Edinburgh, UK EH14 4AS*
[c]*Paramins, Exxon Chemical Ltd., Milton Hill, Abingdon, Oxfordshire, UK OX13 6BB*

High-resolution X-ray powder diffraction using synchrotron radiation has been used to determine the unit-cell parameters of binary (n-$C_{20}H_{42}$/n-$C_{21}H_{44}$ and n-$C_{20}H_{42}$/n-$C_{22}H_{46}$), tertiary (n-$C_{19}H_{40}$ to n-$C_{21}H_{44}$ and n-$C_{20}H_{42}$ to n-$C_{22}H_{46}$) and quinternary (with alkanes ranging from n-$C_{18}H_{38}$ to n-$C_{26}H_{54}$) n-alkane mixed homologous systems, together with a number of real diesel waxes. The structures have been found to conform to the orthorhombic structure with four molecules per unit cell and space group *Fmmm* predicted by Luth *et al.*[8] for binary mixtures. Line profile analysis of the powder patterns revealed the existence of incipient end-chain and interchain disorder; a crystal packing model consisting of interchain mixing, end-chain twisting and chain migration is proposed to account for the observed disorder.

For a broad spectrum of natural linear-chain molecular systems the occurrence of polydispersed aggregates is much more common than the existence of pure compounds: for example, wax fractions from petroleum, linear polymers and biological lipids. For multicomponent *n*-alkane solid-state systems, from a comprehensive literature review published by Mnyukh,[1] rules were formulated to define conditions favourable for the existence of stable solid solutions. It was stated that the addition of a solute molecule A to the solvent B should not increase the space group symmetry. Furthermore, the molecular volumes of the two species should nearly be the same. While these rules seemed to hold for many paraffin solid solutions, there are examples where the existence of an apparently stable solid solution contradicts the constraints placed on unit cell symmetry, in particular.

A number of studies have been undertaken to investigate the ability of *n*-alkanes to form polydispersed crystalline aggregates using calorimetry,[2–4] powder X-ray diffraction techniques,[5–12] X-ray and surface tension measurements,[13] electron diffraction,[4,14–18] FTIR spectroscopy[19] and atomic force microscopy.[15] Studies of the binary mixtures of alkanes have shown that in the liquid state all chain lengths are fully miscible, but in the solid phases the miscibility is strongly influenced by the carbon number difference and odd–even carbon number effects. An additional general feature of binary mixtures is that they often assume untilted orthorhombic structures when the pure components are tilted (likewise for multicomponent mixtures[14]). The studies have also shown that, despite the different chain lengths in the lamellae, the lamella surface is still ordered enough to allow for further nucleation of subsequent layers. Models involving either translational or conformational disorder along the 001 plane have evolved to try and account for this process: however, the exact mechanism for crystallisation is still not fully understood.

In a previous paper,[20] as a step towards understanding the crystallisation process of these multihomologous paraffin systems, we presented our investigations into the structures of some *n*-alkanes within the homologous series $C_{13}H_{28}$ to $C_{60}H_{122}$ using high resolution synchrotron X-ray powder diffraction. In this we found that, in the solid state, in agreement with the broad conclusions of Luth *et al.*,[8] the *n*-alkanes (C_nH_{2n+2}) in general adopt three structurally distinct groups; triclinic [$12<n$(even)<26], orthorhombic [n(even)$\geqslant 36$ and n(odd)] and monoclinic [$28<n$(even)$\leqslant 36$]. These materials crystallise in the form of thin plates with regular faces in which the chain direction is more or less perpendicular to the lamella surface. Prior to melting the alkanes are known to exhibit solid–solid phase transitions to crystalline 'rotator' phases.[21] In the low temperature phase (phase I) the chains adopt the overall *trans* configuration, after which the material may transform to a rotator phase (phase II) in which the chains undergo hindered rotation about the main carbon axis and the molecules are hexagonally packed. Such a transformation is accompanied by an introduction of *gauche* bonds into an otherwise all *trans* structure.[19] Employing line profile analysis, we also found evidence for a degree of structural disorder along the crystallographic *c*-axis for the longer homologues which, we suggested, implied that the process of end-chain bending/folding found in polyethylenes and in *n*-alkanes with a chain length greater than 102 carbon atoms[22,23] was, to a lesser extent, incipient in these systems.

In this paper we present crystallographic high resolution synchrotron X-ray diffraction data on a number of binary, tertiary and quinternary mixed homologue wax systems. The single homologues used to prepare the mixtures ranged from $C_{18}H_{38}$ to $C_{26}H_{54}$: these were selected to represent an average carbon length present within 'real' diesel systems. Together with this, we also present data on a number of real diesel waxes containing a range of average carbon chain lengths. In addition to refined unit cell parameters a number of benchmarking parameters were extracted from the preparation and X-ray data notably the impurity iso-paraffin content, amorphorous content, as well as correlation of the deviation of *c* lattice parameter from ideality to:

- the average carbon number for the *n*-alkane distribution
- the variance of the carbon number distribution
- the thermal disorder [as expressed *via* an isotropic (Wilson factor U^2)]

† now at Blacksmith (A Division of Champion Blacksmith), Minto Ave., Aberdeen AB1 4JZ, UK

● the lattice strain to the planes as calculated from line profile analysis.

The overall strategy was a combinatorial one where qualitative and quantitative indicative parameters are combined in a self-consistent manner producing a solid-state structural model which rationalises the behaviour of wax systems ranging from simple binary mixtures to complicated multihomologous real diesel wax systems. The overall aim of this is to characterise, and account for, the nature and stability of the solid-state structures formed.

Experimental

Sample preparation

The *n*-alkanes used in the preparation of the homologous mixtures were purchased from Aldrich: the purities were all stated as being >99%. Samples for X-ray analysis were prepared by recrystallisation from the melt or twice from *n*-dodecane followed by removal of solvent by placing the sample between absorbent paper and applying pressure for a period of several days. Real diesel wax samples were supplied by Exxon Chemical Ltd. These samples had been crystallised from diesel and were not further prepared in any way. The composition of all samples were determined by gas chromatographic analysis on an HP 5890 gas chromatograph.

Synchrotron X-ray powder diffraction

Powder diffraction patterns were collected using beamlines 8.3 and 2.3[24] at Daresbury synchrotron radiation source. The instrument employed on these two beamlines was the identical two-circle diffractometer providing an incremental angular precision of $\pm 0.0001^\circ$ and an overall angle measuring accuracy of 0.004°. The patterns were recorded using $\theta/2\theta$ geometry with 2θ ranging from 2 to 95° in steps of 10 millidegrees. The data were collected after a number of experimental sessions with wavelength use varying, session to session, within the 1–2 Å range. The wavelength and zero point corrections were refined from the positions of the first five peaks observed for a silicon standard and this resulted in a wavelength accurate to 0.00003 Å and a zero-point accuracy in 2θ of 0.0001°. Diffraction scans were recorded with a rotating sample in order to average out the effects of preferred sample orientation. With the exception of diesel waxes 80441/92-18, 80079/87-11 and 80308/90-112, whose measurements were carried out at low temperatures maintained using a variable-temperature cell,[25] all measurements were carried out under ambient temperatures.

Data reduction and analysis

Unit cell indexing. The data were normalised using the PODSUM program.[26a] The peak shapes and resulting peak positions were fitted using a pseudo-Voight function with the PKFIT program.[26a] The unit cell was indexed from the peak positions using the ITO program[27] which is specifically optimised for indexing powder patterns taken from materials having low-symmetry crystal structures. This program provides a figure of merit (F_m) describing the accuracy of the fit to the proposed unit-cell lattice parameters. This is given by eqn. (1)

$$F_m = \sum_{l=1}^{n} (Q_{obs} - Q_{calc}) / \sum_{l=1}^{n} (Q'_{obs} - Q'_{calc})\ l=1\ l=1 \qquad (1)$$

where Q is the magnitude of reciprocal lattice vector for each peak as defined by eqn. (2),

$$(2 \sin \theta/\lambda)^2 = 1/d^2 = Q \times 10^{-4} \qquad (2)$$

where d is the lattice plane spacing and Q'_{obs} and Q'_{calc} are, respectively, the observed and calculated values for the system. Q_{obs} and Q_{calc} are the same values but for an arbitrary system with the same size reciprocal lattice and n is the number of peaks. A successful indexing is defined by the number of peaks indexed from the first 20 observed and requires the difference between the observed and calculated positions to be $<0.03^\circ$. Following indexing a final refinement of the unit-cell parameters were made using the REFCEL program.[26a]

Previous studies[12,28] suggested that the existence of conformational disorders, arising from the presence of chains with different lengths, is most evident along the crystallographic *c*-axis direction. In this study we monitored the degree of positional disorder in the (001) plane using line profile analysis of the 00l reflections to determine the lattice strain and the isotropic thermal parameter using Wilson's method.[29]

Calculation of lattice strain. Determination of lattice strain effects in the broadening of line profiles was carried out using a simplified method of integral breadths,[30] a modification of the Williamson and Hall[31] approach. In the strain analysis the peak shapes of the 00l reflections were fitted using a pseudo-Voight[32] function with the PKFIT program. In the use of Voightian profiles this method is based on the assumption that the broadening profile due to strain effects is Gaussian and size effects Lorentzian. Furthermore, since all the particles under analysis were very large, then it was assumed that any strain dependent profile broadening resulted from crystalline molecular disorder and not grain size.

An approximation of the lattice strains along the (001) plane of the multihomologous mixtures and real waxes studied was obtained using the relationship[30] in eqn. (3),

$$1/(\delta s) = L - [4 \sin \theta_0/\lambda(\delta s)]^2 e^2 L \qquad (3)$$

where L is the volume-weighted average effective crystallite size along $[hkl]$, e is the upper limit for lattice distortions (lattice strain) and δs is the experimentally derived integral breadth.

Wilson's method. In order to provide a benchmark parameter for statistical disorder, an isotropic temperature factor was estimated from the powder data using Wilson's method.[29] In this, the fall-off of the intensity of the harmonic series of well resolved 001 reflections was examined with respect to 2θ. An isotropic thermal parameter U was calculated using the relationship in eqn. (4),

$$\ln I_{obs} = \ln C - 4\pi^2 U^2 Q \qquad (4)$$

where C is a constant. In this work, the calculated thermal parameter was used as a benchmark to assess whether positional or conformational disorder is brought about by the size differences in chain length mismatches and the number of varying chain lengths.

Amorphous content estimations. An examination of the amorphous content, from the powder patterns of the systems studied, was also carried out in order to generate a comparative model that could identify samples exhibiting poorer crystalline order. The amorphous content is represented by a diffuse halo at the bottom of a set of diffraction peaks, corresponding to an average *d*-spacing of 4.5 Å (see Fig. 1) which roughly corresponds to the inter-chain separation in *n*-alkanes. The method of analysis involved normalising sample diffraction patterns against the (111) diffraction peak using the PLOTEK program.[26b] Once the main diffraction peak had been normalised, the integrated area under all the broad scattering features which reflect scattering from the amorphous regions were calculated. This was used as a qualitative benchmark expressed as a percentage of amorphous to crystalline fractional intensity for assessing relative amorphous content from sample to sample. Variation in (111) peak intensity, sample to sample, was not considered in this analysis.

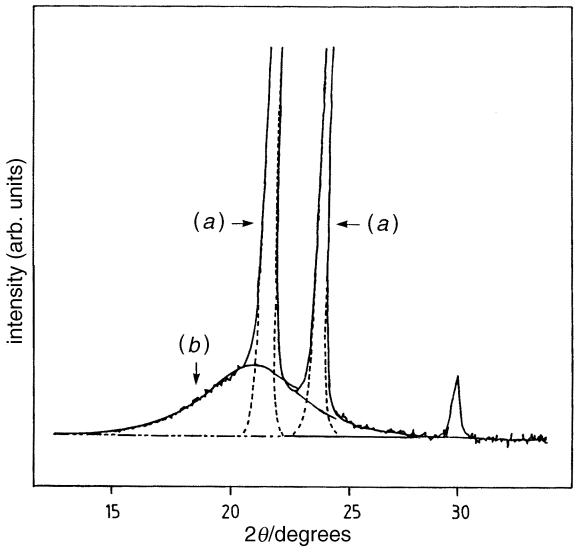

Fig. 1 Plot of a typical wide angle scattering diffraction pattern for a wax indicating the two different regions: (*a*) sharp crystalline diffraction profile and (*b*) broad amorphous halo diffraction profile

Difference length calculations. The calculation of the difference length value is based upon information derived from the X-ray diffraction data and that taken from gas chromatographic traces. Firstly, the cell edge calculated from the indexed lattice parameters describes the actual cell edge length for a sample (average length of the *c*-axis backbone). Secondly, the average carbon number of the *n*-alkanes can be derived from the gas chromatograph by calculating the area under each of the retention peaks for the *n*-alkanes, and subsequently arriving at a weighted average value of *n*-alkanes present. Using eqn. (5) below, a theoretical *c*-axis value can be calculated using the newly derived carbon number average, whereby this should relate to the expected value. This can only be true if the wax structure was held within an ideal packing arrangement (*i.e.* to that of a pure *n*-alkane).

Using the end-group gap of 4.5 Å reported by Stokhuyzen,[33] the average number of carbon atoms per molecule, *n*, was calculated from eqn. (5).

$$c/2 = 1.27(n-1) + 4.5 \quad (5)$$

The difference between the observed and theoretical cell edge will indicate the extent of non-ideal packing that has formed for a particular wax system.

Results and Discussion

Solid solutions of even–even and even–odd binary mixtures

In order to study the solid state structure of *n*-alkane mixtures of even–even and odd–even homologues crystallised from dodecane, X-ray powder diffraction patterns were recorded of mixtures of $C_{20}H_{42}$ with $C_{21}H_{44}$ or $C_{22}H_{46}$. Gas chromatographic analysis revealed the relative impurities for the even–odd mixtures comprised negligible neighbouring homologues, whereas the even–even mixtures were found to contain a maximum of 9.5% dodecane. The resultant X-ray powder diffraction patterns proved to be complicated due to the high density of peaks combined with, in some systems, the presence of multiple phases within the crystal structures formed (see Fig. 2). Refined unit cell parameters determined from the data, together with the final mole ratios of the systems studied, are given in Table 1.

It is evident that all the binary mixtures crystallise to form orthorhombic lattices. The similarity between the *a* and *b* parameters for all the systems indicates that the structures are isostructural; the *c* parameter increases as the percentage of the longer homologue in the sample increases. The systematic absences observed in the powder diffraction patterns for the samples analysed were (*hkl*): $h+k$, $k+l$, $l+h=2n+1$, which is consistent with the orthorhombic structure of space group *Fmmm* with four molecules per unit cell proposed by Luth *et al.*[8] for the high temperature (β_0) phase of binary mixtures. In order for an orthorhombic unit cell containing a mixture of even and odd *n*-alkanes to conform to a *Fmmm* space group there must be at least two-fold disorder of each alkane molecule so that each molecule then has an internal symmetry of *mmm*. Luth[8] suggested that this disorder is brought about by motion induced by heating of the molecules within the lattice structure, that is, the disorder is dynamic.

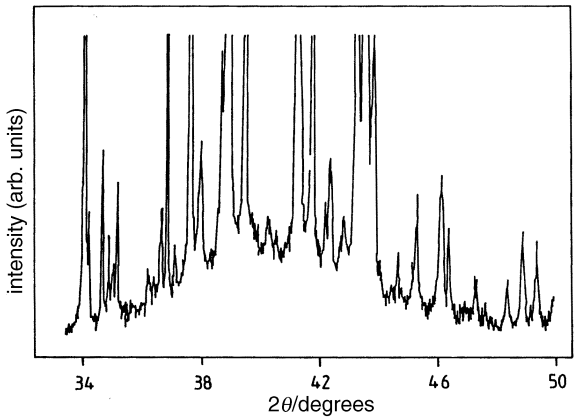

Fig. 2 The central section of a powder diffraction pattern of a sample containing $C_{20}H_{42}$(18%)/$C_{22}H_{46}$(82%) which has been recrystallised twice from $C_{12}H_{26}$. This illustrates the possible profusion of peaks in powder diffraction patterns of mixed phase samples.

Three phases, each of which is orthorhombic, are exhibited within the structure of the even–even binary mixtures when the percentage of the longer homologue exceeds 60%; such behaviour is not evident in similar mixtures crystallised from the melt.[8,34] The exact nature of the orthorhombic structures present in each phase differ: it is suggested that the different phases correspond to microcrystalline segments within the wax mixture induced into the high and low temperature orthorhombic states.

Solid solutions of tertiary and quinternary mixtures

X-Ray powder diffraction patterns were obtained for tertiary mixtures of $C_{19}H_{40}$ with $C_{20}H_{42}$ and $C_{21}H_{44}$, and $C_{20}H_{42}$ with $C_{21}H_{44}$ and $C_{22}H_{46}$, along with quinternary mixtures with alkanes ranging from $C_{18}H_{38}$ to $C_{26}H_{54}$. Gas chromatograhic analysis indicated a relatively low impurity content within each of the systems studied (see Table 1, column 5). The refined unit cell parameters determined from the data, together with the final mole ratios of the systems studied, are given in Table 1.

In all cases only a single structural phase is formed within the solid solutions of the mixed alkanes. The lattice parameters recorded for the mixtures were again found to be orthorhombic structures of space group *Fmmm*, with unit cells similar to that of the binary mixtures. The similarity between the powder diffraction profiles also indicates that the structures are isostructural.

Crystal packing model for multihomologous wax systems

While the structural characterisation has been clarified whereby all the wax mixtures are found to pack in an orthorhombic manner, there still exists a lack of fundamental knowledge as to the exact nature of the packing in relation to the composition. Single odd *n*-alkanes crystallise to form an orthorhombic structure of space group *Pbcm*[20] and, as has been shown, the multihomologous mixtures crystallise to form an orthorhombic

Table 1 Unit cell parameters, figure of merit (F_m) and molecular volumes (V_m) for the homologous mixtures of *n*-alkanes; plus the percentage impurity content present within the mixture (obtained from GC)

no. of components	C_n range	mole ratio	mean C_n	(%) impurity	a/Å	b/Å	c/Å	F_m	V_m/Å^3
2	20,21	69 : 31	20.31	0.0	5.021 (0.003	7.707 0.003	55.910 0.01)	5	2164
		64 : 36	20.36	0.0	5.055 (0.003	7.643 0.004	56.142 0.03)	6	2168
		47 : 53	20.53	0.0	5.109 (0.002	7.630 0.002	56.462 0.01)	6	2200
		40 : 60	20.60	1.0	5.055 (0.001	7.463 0.008	56.405 0.001)	5	2127
		26 : 74	20.74	1.24	5.111 (0.003	7.624 0.003	56.826 0.016)	5	2213
		15 : 85	20.85	0.0	5.027 (0.003	7.617 0.003	57.079 0.018)	6	2186
		9 : 91	20.91	0.0	5.059 (0.002	7.619 0.002	57.056 0.013)	7	2199
		5 : 95	20.95	0.0	5.014 (0.003	7.631 0.009	57.093 0.015)	5	2183
		1 : 99	20.99	0.0	5.064 (0.002	7.461 0.002	57.074 0.012)	10	2156
2	20,22	67 : 33	20.66	0.0	5.026 (0.004	7.691 0.01	57.022 0.03)	5	2204
		64 : 36	20.72	0.0	5.044 (0.003	7.670 0.003	57.474 0.03)	7	2224
		40 : 60	21.20	0.26	5.036 (0.002	7.619 0.001	58.522 0.01)	5	2244
		28 : 72	21.44	1.22	5.180 (0.001	7.192 0.001	55.733 0.002)	5	2076
					5.603 (0.002	7.622 0.001	58.664 0.010)	5	2505
					5.771 (0.002	7.648 0.001	59.287 0.011)	5	2555
		18 : 82	21.64	8.68	5.783 (0.001	7.617 0.001	59.220 0.001)	5	2608
					5.663 (0.002	7.478 0.001	58.207 0.011)	5	2465
					5.095 (0.001	7.182 0.001	55.739 0.005)	5	2040
		14 : 86	21.72	9.53	5.655 (0.002	7.938 0.002	59.438 0.012)	5	2668
					5.604 (0.004	7.618 0.003	58.287 0.048)	5	2488
					5.409 (0.001	7.181 0.001	55.737 0.001)	5	2165
3	19,20,21	6 : 85 : 9	20.83	1.82	5.083 (0.003	7.700 0.006	55.258 0.04)	6	2164
		10 : 66 : 24	20.14	1.26	5.027 (0.0006	7.694 0.0008	55.534 0.01)	28	2148
		13 : 44 : 33	20.30	0.34	5.024 (0.0006	7.696 0.0009	55.985 0.005)	32	2164
		19 : 21 : 60	20.41	0.0	5.025 (0.0004	7.688 0.0005	56.307 0.005)	25	2176
3	20,21,22	8 : 38 : 54	21.46	8.57	5.152 (0.001	7.520 0.001	59.004 0.011)	11	2269
		12 : 67 : 21	21.09	0.0	5.000 (0.001	7.487 0.001	57.917 0.003)	4	2168
		13 : 37 : 50	21.37	0.0	5.159 (0.002	7.635 0.003	58.650 0.016)	4	2310
		0 : 38 : 62	21.62	0.0	5.145 (0.002	7.671 0.001	59.140 0.010)	10	2333
5	18–22	1 : 5 : 12 : 22 : 60	21.35	0.0	5.025 (0.002	7.656 0.004	58.771 0.05)	8	2308
	19–23	6 : 12 : 20 : 30 : 32	21.70	1.18	5.021 (0.002	7.666 0.003	59.928 0.03)	5	2260
	20–24	3 : 10 : 21 : 31 : 35	22.85	0.35	5.250 (0.002	7.143 0.003	62.952 0.017)	6	2360
	21–25	2 : 9 : 2132 : 36	23.91	0.58	5.115 (0.002	7.334 0.002	65.825 0.014)	5	2470
	22–26	6 : 13 : 23 : 29 : 29	24.62	0.78	4.984 (0.002	7.481 0.002	67.869 0.012)	5	2530

structure of space group *Fmmm*. A comparison of the molecular volumes obtained for the crystalline homologous mixtures with those obtained for the single odd *n*-alkanes within the same average carbon chain length range, that is, $C_{19}H_{40}$ to $C_{25}H_{52}$ (see ref. 20), reveals that the unit cells formed by the single odd *n*-alkanes are more densely packed than for any of the homologous mixtures. This point is perhaps obvious if we consider that the single alkane structure has little or no disorder (*i.e.* it is ideally packed) whereas the *Fmmm* structure does have inherent disordered packing constraints. This

disorder will be most evident at the lamellae region where the existence of chain length mismatches will affect the lamellae packing arrangement. To determine the extent and nature of the non-ideal packing along the lamellae (001) plane, a number of the mixed homologue systems were further analysed.

Fig. 3 highlights the proportional relationship that exists between the experimentally observed *c*-axis cell length for the homologous mixture solid solutions formed and the average carbon number. The series of points do not correspond to a truly proportional relationship, as the graph can be seen to curve away as the carbon number average increases. There also exists a degree of scatter and, although this relationship can be seen to be linear, a least-squares fit line emphasises that there still exists a degree of diversity which as yet remains unexplained through any physical or structural rationalisation. The graph also illustrates the extent of non-ideal packing exhibited by these systems; the expected *c* axis lengths determined theoretically using eqn. (5) are greater than the actual values. This difference in length is tabulated in Table 2 and is used as a benchmark to allow for a qualitative comparative analysis of the packing behaviour of the different mixed systems.

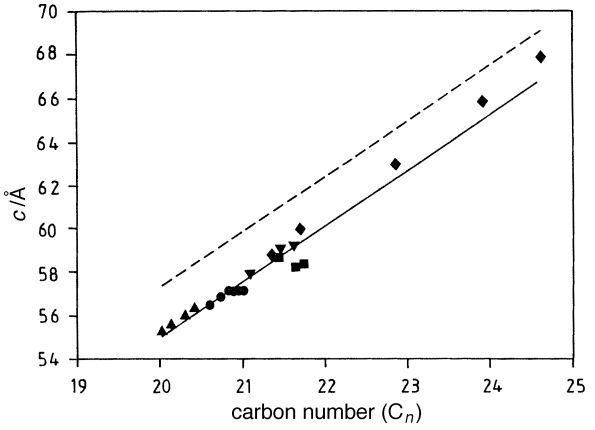

Fig. 3 Plot of average carbon number (C_n) as a function of the *c*-axis parameter for (●) n-$C_{20}H_{42}$/n-$C_{21}H_{44}$, (■) n-$C_{20}H_{42}$/n-$C_{22}H_{46}$, (▲) n-$C_{19}H_{40}$/n-$C_{20}H_{42}$/n-$C_{21}H_{44}$, (▼) n-$C_{20}H_{42}$/n-$C_{21}H_{44}$/n-$C_{22}H_{46}$ and (◆) quinternary alkane mixtures recrystallised from $C_{12}H_{26}$. Solid line is the actual *c*-axis length, while the dashed line represents the expected *c*-axis length.

Disorder arising from the chain length mismatches is one of the factors thought to affect the packing behaviour and stability of the solid solutions formed from the co-crystallisation of the different alkane homologues. Fig. 3 and Fig. 4(*a*) indicate that as the average carbon chain length increases, and as the number of components in the mixed wax systems increases, the difference length decreases.

It has been suggested that the variance (measure of the chain length distributions) will control the stability of the wax produced. A plot of variance *versus* the difference length for each of the wax systems [Fig. 4(*b*)] reveals that as the size of the chain length mismatches (variance) increase the difference length decreases. While there does exist a large degree of scatter in the plot the resulting pattern does perhaps suggest that the ideal *c*-cell length is approached as the number of different homologues present within the solid solution increases. A similar pattern is displayed for the Wilson parameter (U^2) [Fig. 4(*c*)] and the lattice strain along the (001) plane [Fig. 4(*d*)]: as the number of homologues increase in a mixture there is an increase in incipient conformational disorder and lattice strain, and a decrease in the difference lengths.

These results can be rationalised if we consider the different packing arrangements that would arise at the inter-lamellae region as the size of chain length mismatches increases. The packing behaviour of a molecule in a single alkane (zero variance) crystalline system can be easily characterised as an alignment of the end chain methylene groups into a region or gap in between the head and tail of the stacked molecules. This produces a well defined lamellae region[35] as observed in Fig. 5(*a*). Mixtures of *n*-alkanes with low variance (small chain length mismatches) will exhibit similar packing behaviour resulting in low disorder at the lamella interface (see Table 2). As the chain length mismatches increase to two or more carbon atoms the chain ends protruding into the interlamellae region will try and enter the thermodynamically more stable crystalline environment *via* void filling in adjacent lamellae, *i.e.* interchain mixing [Fig. 5(*b*)]. In this, the all-*trans* backbone structure of the alkane chain will be maintained resulting in very little conformational disorder (reflected in a low Wilson parameter); there will, however, be an increase in the disorder of the lamellae region (seen as an increase in the overall percentage disorder—Table 2).

Table 2 Calculated physical parameters for the homologous mixtures of *n*-alkanes co-crystallised from dodecane; difference length, variance (V_n), thermal parameter (U^2), relative strain and relative percentage disorder

no of components	C_n range	mean C_n	difference length/Å	V_h	U^2/Å^2	rel. strain	disorder (%)
2	20,21	20.60	0.94	0.24	2.163	1.000	3.24
		20.74	0.91	0.19	1.560	0.491	2.45
		20.85	0.92	0.13	1.495	1.553	3.03
		20.91	0.99	0.08	1.093	1.127	3.03
		20.95	1.02	0.05	1.155	0.959	3.54
		20.99	1.06	0.01	1.213	1.066	—
2	20,22	21.44	0.88	0.81	1.404	0.138	11.64
		21.64	0.87	0.59	1.830	0.724	5.17
		21.72	0.86	0.48	1.684	0.855	1.40
3	19,20,21	20.03	0.818	0.15	3.510	0.751	25.47
		20.14	0.82	0.32	3.704	1.194	10.0
		20.30	0.80	0.47	3.369	1.108	74.49
		20.41	0.79	0.62	4.371	1.652	16.41
3	20,21,22	21.46	0.77	0.41	2.287	2.029	3.73
		21.09	0.83	0.32	1.571	1.175	3.33
		21.37	0.82	0.49	2.268	0.901	4.23
		21.62	0.88	0.24	1.600	0.497	2.51
5	18–22	21.35	0.76	0.89	2.920	8.393	16.11
	19–23	21.70	0.65	1.45	3.943	3.254	35.16
	20–24	22.85	0.61	1.21	2.973	5.502	3.41
	21–25	23.91	0.54	1.10	3.164	5.226	1.74
	22–26	24.62	0.44	1.44	—	—	1.88

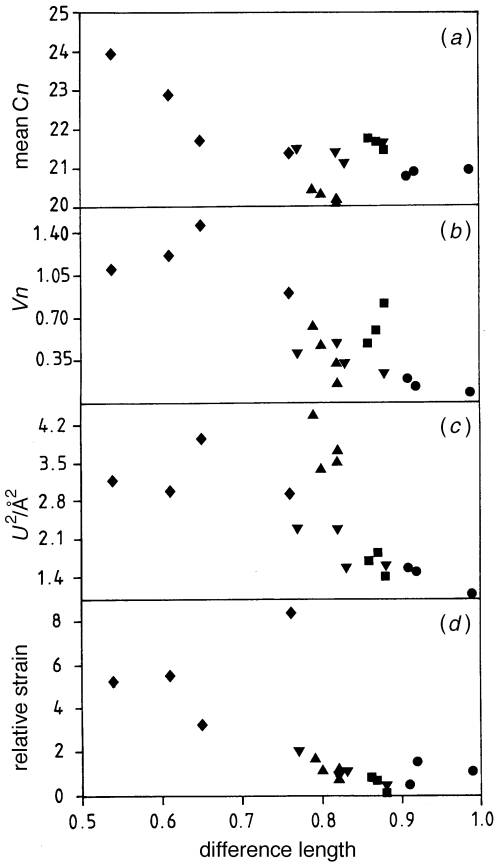

Fig. 4 Plot of (*a*) carbon number average, (*b*) variance, (*c*) Wilson parameter (U^2) and (*d*) lattice strain along the [00l] plane for (●) *n*-$C_{20}H_{42}$/*n*-$C_{21}H_{44}$, (■) *n*-$C_{20}H_{42}$/*n*-$C_{22}H_{46}$, (▲) *n*-$C_{19}H_{40}$/*n*-$C_{20}H_{42}$/*n*-$C_{21}H_{44}$, (▼) *n*-$C_{20}H_{42}$/*n*-$C_{21}H_{44}$/*n*-$C_{22}H_{46}$ and (◆) quinternary alkane mixtures recrystallised from $C_{12}H_{26}$.

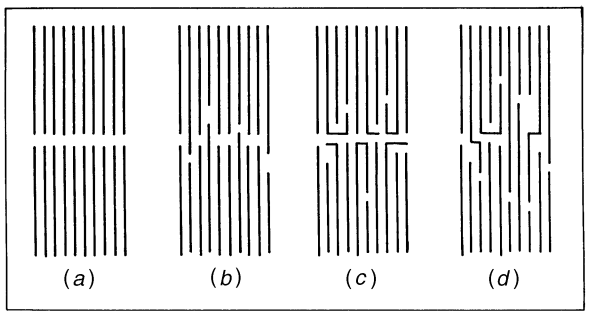

Fig. 5 Schematic representation of interlamellae packing for (*a*) single alkane exhibiting a well ordered lamellae region, (*b*) low variance alkane mixture undergoing interchain mixing, (*c*) high variance alkane mixture exhibiting end-chain twisting and folding disorders and (*d*) combined interchain mixing and end-chain bending/twisting disorders at the lamella interface

As the chain length mismatches increase to three or four carbon atoms difference, disorder results at the lamellae interface as alkane chain ends protrude into the interlamellae region. These chain ends, no longer held by the constraints of the adjacent van der Waals forces, would be able to twist and fold back into the crystal lattice resulting in conformational disorder (deviations from the all-*trans* structure) at the lamellae interface [Fig. 5(*c*)]. While such conformational disorders are thermodynamically less favourable than the all-*trans* structure they are necessarily introduced in order to enhance the stability of the solid solution formed. The re-entering chains would also cause an increase in strain along the [001] plane as they push parallel packed chains apart as they strive to re-enter the stability of the crystalline lattice. The increased disorder in the interlamellae region resulting from the presence of chain twists and folds trying to accommodate within the lamella packing would result in an increased interlamellae spacing and thus higher *c*-cell lengths than for the lower variance systems.

The proposed model would be consistent with the results obtained: lamella packing in the low variance systems dominated by interchain mixing and the higher variance systems with chain folding and twisting. It is likely, however, that while each system may be dominated by one process over another, both processes will probably be in operation simultaneously in varying degrees in each system [Fig. 5(*d*)]. Previous studies employing FTIR spectroscopy on solid solutions of multihomologous mixtures[9,19] have also shown the existence of conformational disorders in such systems.

Solid solutions of real diesel wax systems

In order to determine a crystal packing model for real diesel waxes X-ray powder diffraction patterns were recorded for a number of wax-crystallised diesel fuel extracts of varying carbon number range and variance. Gas chromatographic analysis revealed that the waxes displayed the typical Gaussian distribution of *n*-alkanes traditionally observed for fuel-crystallised systems, enabling the characterisation of the wax materials (see Fig. 6). In addition to the *n*-alkanes, a minor series of methyl-branched alkanes is also observed indicating the existence of an iso-paraffin impurity present within the fuel systems.

The lattice parameters determined for the wax samples filtered from diesel fuels are given in Table 3. Most of the waxes were indexed using the program ITO. A number of the poorer crystalline materials possessed less than 20 diffraction peaks, which was below the minimum number of peak positions required to generate a lattice parameter, whereby a figure of merit would not be obtained. In these cases an estimate was made as to the correct index for the remaining peaks (using an indexed wax as a model comparison) and the unit cell parameters were refined using REFCEL.

Lattice parameters for the wax materials were, like in the multihomologous mixtures, all found to be orthorhombic with four molecules per unit cell. The *c*-axis parameter (Fig. 7) and molecular volume were both found to increase linearly with average carbon number. A two phase system was also found to appear in the real diesel waxes assumed to relate to regions with differing packing arrangements, whereby the phase behaviour can be seen to correlate directly with the average carbon number of the wax. The higher melting point waxes (or higher

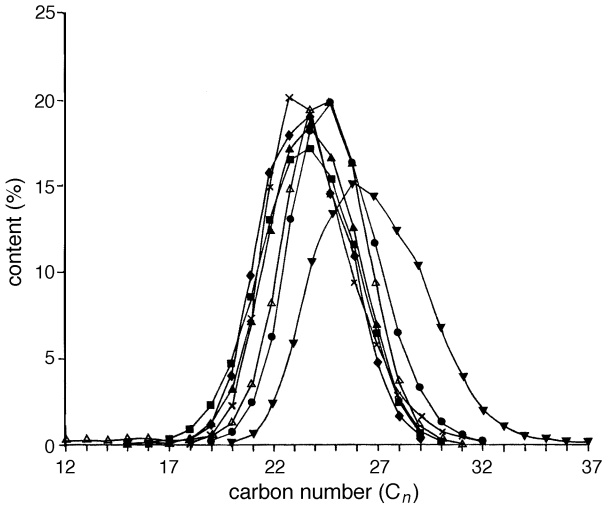

Fig. 6 Carbon number distribution plot for a range of waxes crystallised from real diesel obtained from a high temperature GC capillary column; C_n=(◆) 23.57, (■) 23.66, (▲) 33.92, (x) 23.93, (△) 24.36, (●) 25.05 and (▼) 26.80. Average carbon number range: $20.72 \leqslant C_n \leqslant 22.53$.

Table 3 Unit cell parameters, figure of merit (F_m), crystal phase (β—low temperature, β_0—high temperature) and molecular volumes (V_m) for the real diesel waxes; plus the percentage iso-paraffin content present within the wax system (obtained from GC)

wax type	C_n range	mean C_n	iso-paraffin (%)	a/Å	b/Å	c/Å	F_m	V_m/Å^3	T/°C	phase
80734/84-24	15–27	19.13	—	4.849 (0.005	8.061 0.005	54.734 0.065)	1.35	2139	22.0	β_0
80441/92-18	15–29	20.11	1.81	4.995 (0.008	7.430 0.006	55.772 0.113)	2.62	2070	−7.0	β
80074/87-11	15–29	20.73	1.20	4.951 (0.001	7.838 0.001	57.709 0.005)	0.09	2239	22.0	β_0
80079/87-11	12–25	20.83	1.04	4.997 (0.001	7.421 0.001	57.580 0.007)	0.14	2135	−7.7	β
80653/90-14	14–29	21.55	1.62	4.991 (0.002	7.738 0.002	60.085 0.021)	0.44	2321	22.0	β_0
80708/89-14	15–30	21.96	2.31	5.020 (0.001	7.648 0.001	61.859 0.011)	0.22	2375	22.0	β_0
80002/88-13	16–28	22.06	1.40	5.025 (0.002	7.629 0.002	60.873 0.018)	0.46	2333	22.0	β_0
80653/90-10	15–29	22.12	2.40	5.013 (0.001	7.673 0.001	61.688 0.004)	0.08	2373	22.0	β_0
80167/88-19	15–31	22.18	1.77	4.981 (0.004	7.753 0.004	61.538 0.063)	1.05	2377	22.0	β_0
80447/87-10	14–29	22.25	2.07	5.022 (0.004	7.642 0.004	62.677 0.051)	0.98	2405	22.0	β_0
TK197-10	12–26	22.27	—	5.030 (0.004	7.625 0.004	62.602 0.045)	1.06	2401	22.0	β_0
TK197-16	17–29	22.35	0.99	5.011 (0.003	7.668 0.003	62.097 0.054)	0.90	2386	22.0	β_0
80308/90-11	17–28	22.54	3.10	5.024 (0.005	7.639 0.005	62.450 0.059)	1.11	2397	22.0	β_0
80308/90-112	17–29	22.59	2.96	4.984 (0.001	7.418 0.001	62.366 0.011)	0.25	2301	−7.0	β
tk186-7a	17–29	22.61	3.15	5.013 (0.001	7.675 0.001	62.465 0.011)	0.28	2403	22.0	β_0
TK186-7b	15–25	22.71	2.95	5.027 (0.002	7.615 0.001	62.758 0.017)	0.41	2402	22.0	β_0
				5.004 (0.005	7.482 0.004	63.584 0.059)	1.38	2381	22.0	β_0
80312/86-13	15–32	22.82	3.39	4.983 (0.011	7.579 0.010	63.055 0.138)	2.93	2381	22.0	β_0
80226/89-16a	18–31	23.36	2.93	5.004 (0.002	7.484 0.002	65.376 0.028)	0.49	2448	22.0	β
80226/86-16	14–32	23.46	3.62	5.021 (0.002	7.624 0.002	63.892 0.028)	0.58	2445	22.0	β_0
80226/86	14–32	23.46	5.38	5.001 (0.002	7.482 0.002	65.268 0.023)	0.50	2442		β
80152/86-16	18–27	23.50	4.65	5.015 (0.002	7.645 0.001	64.531 0.019)	0.44	2474	22.0	β_0
				5.000 (0.001	7.487 0.001	66502 0.011)	0.33	2489		β
80291/87-10	18–29	23.57	2.78	5.001 (0.001	7482 0.001	65.301 0.001)	0.02	2443	22.0	β
80226/89-21	16–30	23.66	2.50	5.000 (0.010	7.482 0.009	66.309 0.126)	2.12	2481	20.0	β
80619/88-8	18–30	23.67	3.06	5.020 (0.002	7.639 0.002	64.739 0.028)	0.50	2483	22.0	β_0
				5.002 (0.004	7.491 0.003	65.620 0.049)	0.85	2459		β
80312/86-8	15–32	23.67	3.35	5.000 (0.001	7.842 0.001	66.126 0.013)	0.29	2474	22.0	β
80619/88-3	18–30	23.69	3.13	5.001 (0.002	7.490 0.002	66.521 0.027)	0.46	2492	22.0	β
80226/86-16c	15–31	23.92	2.34	4.999 (0.002	7.481 0.002	66.421 0.025)	0.42	2484	22.0	β
80442/92 + 5	18–32	23.95	3.92	4.999 (0.003	7.487 0.002	66.111 0.028)	0.44	2474	22.4	β
80312/86-7	17–35	24.20	2.02	4.994 (0.001	7.483 0.001	69.626 0.018)	0.36	2602	22.0	β
80226/89-11	11–31	24.36	1.87	4.993 (0.002	7.483 0.002	67.962 0.027)	0.41	2539	24.0	β
89015/91-14	19–32	25.05	1.89	4.995 (0.001	7.490 0.001	69.132 0.015)	0.29	2586	22.0	β
Para32,720-4	18–32	25.60	2.36	4.989 (0.002	7.480 0.002	75.920 0.032)	0.52	2833	22.0	β
Shell Wax	20–37	26.80	5.98	4.989 (0.003	7.471 0.003	74.147 0.048)	0.82	2764	22.0	β
Para32,721-2	17–34	27.4	4.55	4.986 (0.001	7.476 0.001	80.416 0.020)	0.29	2998	22.0	β
Astor B Wax	21–43	32.06	—	4.980 (0.001	7.455 0.001	90.921 0.024)	0.18	3375	22.0	β

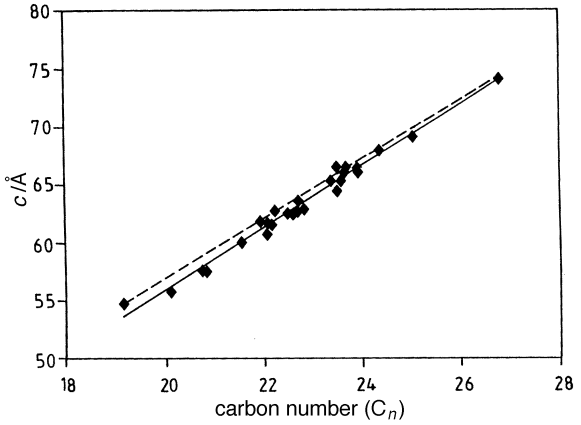

Fig. 7 Plot of average carbon number (C_n) as a function of the *c*-axis parameter for a range of real diesel waxes. Solid line is the actual *c*-axis length, while the dashed line represents the expected *c*-axis length.

average carbon number) maintain their structural integrity at ambient temperatures whereby the lower melting point waxes, which are only partially crystalline, undergo a rotator transition resulting in a phase change. The two phases, identified previously by Luth *et al.*[8] for binary mixtures, were identified as orthorhombic in nature.

Crystal packing model for real diesel wax systems

The crystallinity of a particular wax sample is known to be dependent upon the iso-paraffin content,[36] thermal history,[37] size of chain length mismatches and molecular mass.[5,6] Comparison of the X-ray powder patterns obtained for a single alkane,[20] the homologous mixtures and a diesel wax (Fig. 8) indicates a decrease in crystallinity as the number of components in the system increases. The increase in the fall-off in intensity of the (001) reflections as the range of *n*-alkanes co-crystallising increases, also indicates a growth in the magnitude of the positional disordering along the crystallographic *c*-axis (carbon chain) as observed in the Wilson plots for the various systems (Fig. 9).

As with the multihomologous mixtures, a qualitative comparative approach was taken to determine the nature and extent of the disordered packing for the different wax systems of varying carbon number range and variance. Fig. 7 illustrates the extent the actual *c*-cell parameter lengths observed for the wax systems deviated from the ideal packing length. While the plot does show a degree of scatter, the difference lengths observed for the real wax systems are smaller than those observed for the homologous mixtures.

Table 4 tabulates the experimentally derived physical properties for the wax materials. Plots of difference length *versus* mean carbon chain length, variance, disorder parameter (U^2) and relative strain for the real wax systems (Fig. 10) reveal, unlike for the homologous mixtures, no discernible pattern. Most of the waxes crystallised from the fuels do not have dramatically different carbon number averages or variance values. When comparing systems with such subtly differentiating physical properties, relative to the defect nature of the wax, it would be unlikely that any distinct trends would be observed. Comparing, however, the derived physical values for the waxes with those obtained for the homologous mixtures, it would seem reasonable to suggest that the lamella packing model proposed for the homologous mixtures, consisting of interchain mixing and end-chain deformation, could be applied to the real wax systems. The small difference length observed for the waxes could also be indicative of an interlamellae packing dominated by the chain folding and twisting process, as suggested for the high variance multihomologous systems. FTIR spectroscopic analysis[19,38] of the real wax systems indicate the existence of *gauche* conformers present within the solid solution of the real wax systems. It would be difficult to assert this as definitive evidence for the existence of the end chain distortions solely, as the presence of iso-paraffins, identified from the GCs, would also result in *gauche* conformers and lead to higher disorder parameters.

The diffraction data recorded for the real diesel wax systems indicate the presence of the crystalline phase co-existing with a poorer ordered phase (amorphous type), observed as an amorphous halo at the baseline of the crystalline diffraction

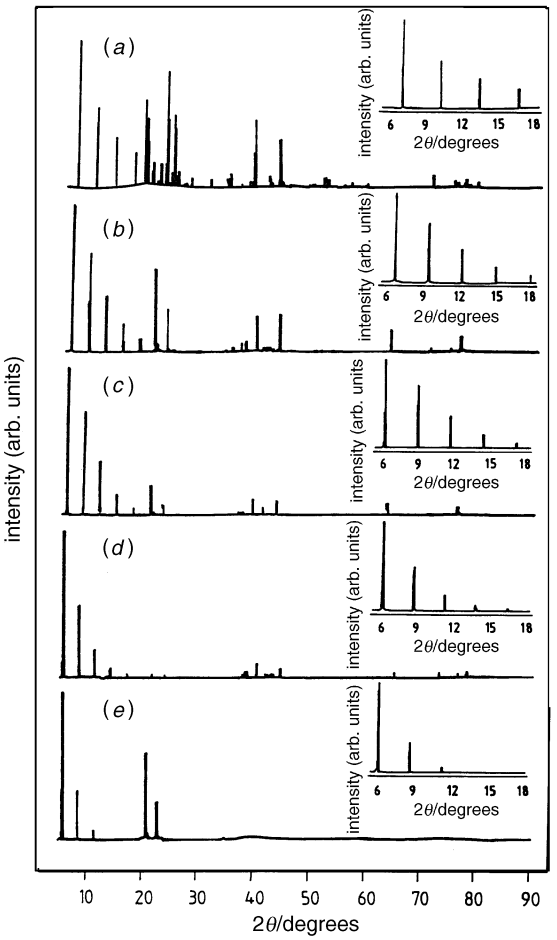

Fig. 8 Comparison of powder patterns obtained for (*a*) *n*-$C_{20}H_{42}$, (*b*) *n*-$C_{20}H_{42}$(26%)/*n*-$C_{21}H_{44}$(74%), (*c*) *n*-$C_{20}H_{42}$(13%)/*n*-$C_{21}H_{44}$(37%)/*n*-$C_{22}H_{46}$(50%), (*d*) quinternary mixture (*n*-$C_{20}H_{42}$ to *n*-$C_{24}H_{50}$) and (*e*) real diesel wax (80002/83-13) [the inset illustrates the (00l) reflections on which line profile analysis was carried out]

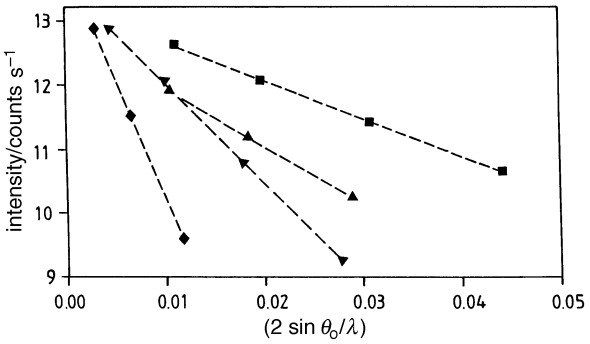

Fig. 9 Wilson plots obtained for (■) *n*-$C_{20}H_{42}$(15%)/*n*-$C_{21}H_{44}$(85%), (▲) *n*-$C_{20}H_{42}$(8%)/*n*-$C_{21}H_{44}$(38%)/*n*-$C_{22}H_{46}$(54%), (▼) five component mixture with alkane range *n*-$C_{19}H_{40}$ to *n*-$C_{23}H_{48}$ and (◆) real diesel wax (Shell) illustrating the increase in the fall-off in intensity of the (00l) reflections with increasing number of components in the solid-solution mixtures

Table 4 Calculated physical parameters for the real diesel wax systems; difference length, variance (V_n), thermal parameter (U^2), relative strain and relative percentage disorder

C range	mean C_n	difference length/Å	V_n	U^2/Å^2	rel. strain	rel. (%) disorder	phase
15–27	19.13	0.12	3.96	6.420	1.792	100.0	β_0
15–29	20.11	0.70	5.50	7.508	1.672	4.91	β_0
15–29	20.73	0.55	5.24	23.501	3.702	60.00	β_0
15–25	20.83	0.70	5.82	9.632	5.026	8.85	β
15–29	21.55	0.44	4.32	22.909	1.821	75.96	β_0
15–30	21.96	0.15	4.34	20.715	4.579	56.54	β_0
16–28	22.06	0.64	2.91	5.230	3.104	86.93	β_0
15–29	22.12	0.38	4.84	21.913	3.895	52.19	β_0
15–31	22.18	0.50	5.46	8.502	1.721	88.23	β_0
14–29	22.25	0.12	4.82	23.418	4.732	54.42	β_0
17–28	22.54	0.50	3.78	19.262	12.395	52.69	β_0
17–29	22.59	0.58	3.83	6.591	1.471	5.07	β
17–29	22.61	0.56	5.87	7.080	1.814	69.89	β_0
15–25	22.71	0.55	3.35	4.811	1.832	53.21	β_0
		0.22	3.35	6.167	1.344	3.33	β
15–32	22.82	0.54	5.26	8.559	10.896	79.71	β_0
18–31	23.36	0.16	4.67	23.117	5.349	9.20	β
18–27	23.50	0.64	4.57	5.691	4.229	13.75	β
18–29	23.57	0.40	3.88	17.407	1.694	5.96	β
16–30	23.66	0.10	5.01	22.828	5.877	7.61	β
15–32	23.67	0.18	5.26	19.944	0.866	9.01	β
18–30	23.69	0.04	3.90	6.693	3.688	6.67	β
15–31	23.92	0.31	4.51	20.874	1.219	6.11	β
18–32	23.93	0.45	4.39	5.207	13.331	3.73	β
11–32	24.36	0.15	5.38	5.606	3.919	4.03	β
19–32	25.05	0.38	4.22	5.561	5.889	3.27	β
20–37	26.80	0.15	7.97	9.444	4.756	9.61	β

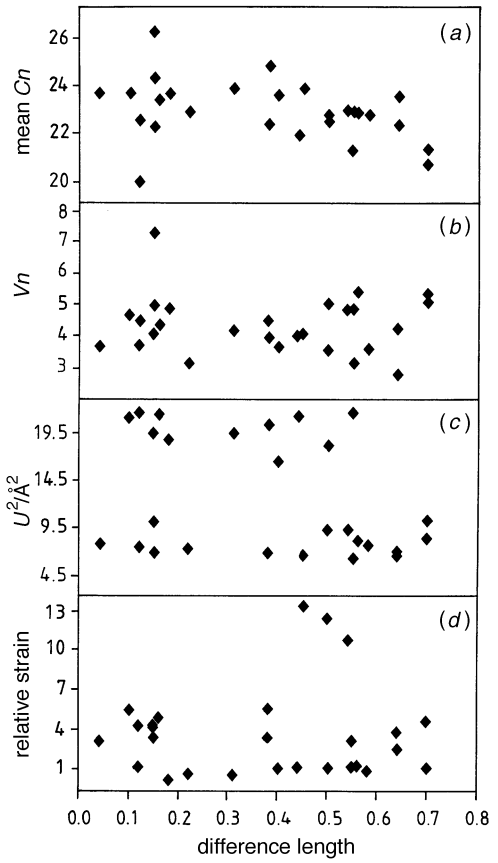

Fig. 10 Plot of (*a*) carbon number average, (*b*) variance, (*c*) Wilson parameter (U^2) and (*d*) lattice strain along the [00l] plane for the real diesel waxes

peaks. Fig. 11 depicts the amorphous peaks displayed in the background diffraction data for the real diesel waxes. The main characteristic peaks appear at about 20, 40 and 77° (2θ) and correspond approximately to *d*-spacings of 4.5, 2.2 and 1.2 ($\pm$0.5) Å. These values roughly correspond to interchain separations of primary, second and third harmonics correlations respectively in the crystalline *n*-alkanes fraction thus implying that disorder in the adjacent chain packing could account for the amorphous nature.

While the disorder parameter (U^2) and the percentage disorder (see Table 4) may be interrelated, the former refers to conformational disorder along a particular axis (carbon chain) and denotes the efficiency of packing within the lamella region, while the latter is based predominantly on the peaks corresponding to the adjacent interchain packing. The inclusion of solvent, iso-paraffins and conformational distortions in the parallel chain packing and interlamellae packing will undoubtedly result in some of the disorder identified in the diffraction patterns. The diffraction profiles relating to the adjacent chain packing do indicate a poorer crystallinity, as many peaks are inadequately resolved and have large peak halfwidths. On comparison, however, of the relative percentage disorder (amorphous content) with the lattice strain and Wilson parameter for the wax crystals (see Table 4), we find that no correlation exists between these parameters. This indicates that the amorphous and crystalline regions are not mutually dependent, and that an increasing amorphous content does not adversely influence the ordered packing within the lattice.

Comparing the relative percentage disorder values with the temperature at which the wax phases are held (Table 4), it is evident that a relationship does exist between these. The solid solutions held within the high temperature crystal phase (β_0) exhibit a far greater amorphous (relative disorder) content than the lower temperature phase (β). It is known the temperature conditions[5] (or thermal history) under which the wax crystals are kept can substantially affect the packing of the *n*-alkanes, which are known to be very mobile well below the melting point. If the sample temperature is raised at any point,

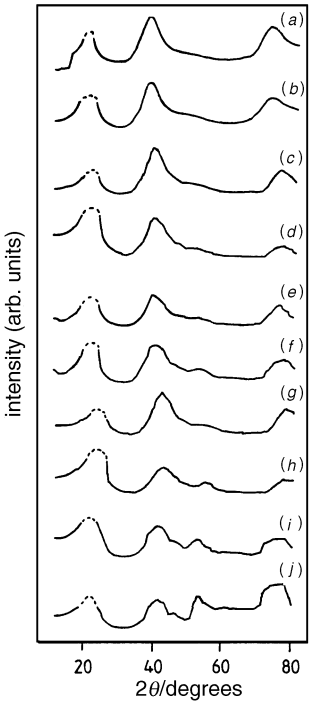

Fig. 11 Comparison of the background amorphous profiles observed in the powder patterns of the real diesel waxes. The plot shows the amorphous profiles obtained for waxes with mean carbon chain lengths (*a*) 0 18.3, (*b*) 21.3, (*c*) 21.5, (*d*) 21.6, (*e*) 22.0, (*f*) 22.7, (*g*) 22.8, (*h*) 23.2, (*I*) 24.7 and (*j*) 26.9.

this will induce molecular migration within the crystal altering the packing stability within; as found for binary mixtures with chain length differences greater than six carbon atoms.[13,16] If the wax crystal is held above the first main rotator transition temperature, this will induce a favourable ordering rearrangement in the lamellae, reducing the overall disorder within this region.

Based on these results and taking into account the external factors that can change or alter the packing, a broader crystal packing model (Fig. 12)—based on the simplified models proposed for the homologous mixtures—is tentatively proposed for the real diesel waxes. The large range of carbon chain lengths present within the wax systems will lead to a large amount of disorder in the lamella region, thus disrupting the interlamellae packing and hindering further nucleation along that plane. The system thus appears to compensate for the chain length mismatches *via* interchain mixing [to lesser (i) or greater degree (ii)] and end-chain twisting (as discussed above) so maintaining the integrity of the lamella interface [Fig. 12(*a*)]. Such processes produce kinks (*gauche* conformers) along the carbon backbone as the lattice pushes apart to accommodate the twisted back and intermixing chains. This overall process results in an increase in the interchain spacing and an increased strain which is observed as a broadening of the (*hk*0) peaks. At higher temperatures (β_0 phase) the molecular mobility of the chains allows for chain diffusion and migration, as chains of similar chain length come together to form thermodynamically more favourable (less disordered) lamella interfaces [Fig. 12(*b*)]. A looser packing arrangement could also be expected to display kinks within the carbon backbone or exist as a separate phase of poorly ordered straight chains that are unable to cocrystallise due to the large chain length mismatches [Fig. 12(*c*)].

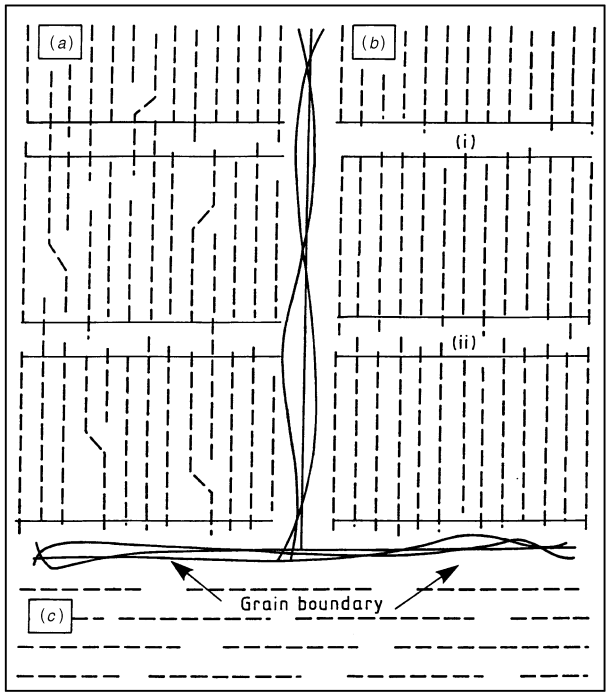

Fig. 12 The packing groups thought to exist within diesel crystallised wax. Region (*a*) represents the regions of high strain resulting from long *n*-alkane protrusions, (*b*) represents the end chain packing of a wax with both types of high and low lamellae disorder and (*c*) demonstrates the presence of amorphous regions possessing no lamellae order with a minimal adjacent chain packing order. The grain boundary also contributes to the amorphous content of the material. Although drawn in this manner there is no requirement to assume orthogonality of regions (*a*) and (*b*) *versus* (*c*). Regions (i) and (ii) refer, respectively, to areas involved in end-chain mixing to a lesser or greater degree.

In summary, the waxes crystallising in the higher temperature (β_0) form pack with a degree of (rotational) disorder. This provides less restriction on molecular migration than the more ordered (β) phase. Thus in the β_0 phase segregation between those chains of similar length (more crystalline fraction) and the residual components (less ordered components) can be expected which perhaps explains the higher amorphous content observed in the samples crystallising in the β_0 phase. This disorder can either be manifested *via* the residual molecular component aligned within the grain boundaries or within the amorphous regions characterised by poorly defined interlaminae regions [*e.g.* Fig. 12(*c*)].

Research towards improving our understanding of the structural aspects of wax crystallisation has been supported for a number of years through research grants from the ESPRC and Exxon Chemical Ltd. We gratefully acknowledge Exxon Chemical Ltd. for the financial support of a studentship (S.R.C.), ESPRC for providing beam time on the Daresbury SRS and for the financial support of a studentship (G.P.H.) and senior fellowship (K.J.R.).

References

1 Y. V. Mnyukh, *J. Phys. Chem. Solids*, 1963, **24**, 631.
2 G. Zerbi, R. Piazza and K. Holland-Moritz, *Polymer*, 1982, **23**, 1921.
3 B. Flaherty, *J. Appl. Chem. Biotechnol*., 1971, **21**, 144.
4 D. L. Dorset and R. G. Snyder, *Macromolecules*, 1995, **28(24)**, 8412.
5 K. E. Russel, B. K. Hunter and R. D. Heyding, *Eur. Polym. J*., 1993, **29**, 211.
6 E. C. Reynhardt, *J. Phys. D: Appl. Phys*. 1986, **19**, 1925.
7 M. Dirand, Z. Achour, B. Jouti, A. Sabour and J. C. Gachon, *Mol. Cryst. Liq. Cryst*., 1996, **A275**, 293.
8 H. Luth, S. C. Nyburg, P. M. Robinson and H. G. Scott, *Mol. Cryst. Liq. Cryst*., 1972, **27**, 337.
9 M. Maroncelli, H. L. Strauss and R. G. Snyder, *J. Phys. Chem*., 1985, **89**, 5260.
10 G. I. Asbach and H. G. Kilian, *Polymer*, 1991, **32**, 3006.
11 D. L. Dorset, J. Hanlon and G. Kavet, *Macromolecules*, 1989, **22**, 2169.
12 I. Denicolo, A. F. Craievich and J. Doucet, *J. Chem. Phys*., 1984, **12**, 80.
13 X. Z. Wu, B. M. Ocko, H. Tang, E. B. Sirota, S. K. Sinha and M. Deutsch, *Phys. Rev. Lett*., 1995, **75**, 1332.
14 D. L. Dorset, *Acta Crystallogr., Sect. B,* 1995, **51**, 1021.
15 D. L. Dorset and B. K. Annis, *Macromolecules*, 1996, **29**, 2969.
16 D. L. Dorset and R. G. Snyder, *J. Phys. Chem*., 1996, **100**, 9848.
17 D. L. Dorset, *Macromolecules*, 1985, **18**, 2158.
18 D. L. Dorset, *Macromolecules*, 1987, **20**, 2782.
19 G. P. Hastie and K. J. Roberts, *J. Mater. Sci*., 1994, **29**, 1915.
20 S. R. Craig, G. P. Hastie, K. J. Roberts and J. N. Sherwood, *J. Mater. Chem*., 1994, **4**, 997.
21 H. E. King Jr., E. B. Sirota, H. Shao and D. M. Singer, *J. Phys. D: Appl. Phys*., 1993, **26**, B133.
22 See A. Keller in; *Sir Charles Frank: An 80th Birthday Tribute,* ed. R. Chalmers, J. E. Enderby, A. Keller, A. R. Lang and J. W. Steeds, Adam Hilger, Bristol, 1991.
23 G. Ungar, J. Stejny, A. Keller, I. Bidd and M. C. Whiting, *Science*, 1985, **229**, 386.
24 R. J. Cernik, P. K. Murrey, P. Pattison and A. N. Fitch, *J Appl. Crystallogr*., 1990, **23**, 292.
25 S. R. Craig, K. J. Roberts, J. N. Sherwood, K. Sato, M. Iwahashi and R. J. Cernick, *J. Cryst. Growth*, 1993, **128**, 1263.
26 (*a*) Powder Diffraction Program Library, CLRC Daresbury Laboratory; (*b*) PLOTEK, Data Acquisition Group; unpublished, CLRC Daresbury Laboratory, Warrington, WA4 4AD.
27 J. W. Visser, *J. Appl. Crystallogr*., 1969, **2**, 89.
28 J. J. Retief, D. W. Engel and E. G. Boonstra, *J. Appl. Crystallogr*., 1985, **18**, 156.
29 G. H. Stout and L. H. Jensen, *X-ray Structure Determination*, Wiley-Interscience, New York, 2nd edn., 1989.
30 S. R. Craig, G. P. Hastie and K. J. Roberts, *J. Mater. Sci. Lett*., 1996, **15**, 1193.
31 G. K. Williamson and W. H. Hall, *Acta Metallurgica*, 1953, **1**, 22.
32 R. A. Young and D. B. Wiles, *J. Appl. Crystallogr*., 1982, **15**, 430.

33 R. Stokhuyzen, *An investigation of the structural problems in relation to some synthetic waxes*, 1969, MSc thesis, Rhodes University, Grahamstown, South Africa.
34 A. R. Gerson, PhD Thesis, *Structural and Kinetic Aspects of the Crystallisation of* n-*Alkanes, Homologous Mixtures and Real Waxes*, University of Strathclyde, Glasgow, 1990.
35 G. Strobl, B. Ewen, E. W. Fischer and W. Pieszcek, *J. Chem. Phys*., 1974, **61**, 5257.
36 R. M. Butler and D. M. MacLeod, *Can. J. Cem. Eng*., 1961, **39**, 53.
37 J. J. Retief and J. H. le Roux, *S. Afr. J. Sci*., 1983, **79**, 234.
38 S. R. Craig, PhD Thesis, *Synchrotron Radiation Studies of the Structure of* n-*Alkanes and Homologous Mixtures*, University of Strathclyde, Glasgow, 1995 p. 152.

Paper 7/06532I; *Received* 8*th September*, 1997